AD-A087 225 GEORGIA INST OF TECH ATLANTA CENTER FOR THE ADVANCEM--ETC F/6 20/11
EFFICIENT COMPUTATIONAL TECHNIQUES FOR THE ANALYSIS OF SOME PRO--ETC(U)
JUN 80 T NISHIOKA, S N ATLURI N00014-78-C-0636
UNCLASSIFIED GIT-CACM-SNA-20 NL

Office of Naval Research

(15) Contract N00014-78-C-0636 NR 064-610

(9) Technical Report No. 4

Report No. GIT-CACM-SNA-20, V 77

(14)

(6) EFFICIENT COMPUTATIONAL TECHNIQUES FOR THE ANALYSIS OF SOME PROBLEMS OF FRACTURE IN PRESSURE VESSELS AND PIPING

by

(10) T. Nishioka and Satya N. Atluri

(11) JUN 80

(12) 92

Center for the Advancement of Computational Mechanics

School of Civil Engineering

Georgia Institute of Technology

Atlanta, Georgia 30332

EFFICIENT COMPUTATIONAL TECHNIQUES FOR THE ANALYSIS OF SOME PROBLEMS OF FRACTURE IN PRESSURE VESSELS AND PIPING

T. Nishioka* and Satya N. Atluri**
Center for the Advancement of Computational Mechanics
School of Civil Engineering
Georgia Institute of Technology
Atlanta, GA 30332

Abstract

Results of (i) a numerical investigation, based on an energy consistent moving-singularity dynamic finite element procedure, of fast crack propagation in a finite plate; (ii) numerical simulation of experimental data on fast crack propagation and arrest in a double-cantilever-beam specimen; and (iii) stress-intensity factor solutions in a thermally shocked cylindrical vessel containing an inner surface (meridional) elliptical flaw, are presented. Comparison of these results with other available solutions, and pertinent discussions, are included.

Introduction

Concise summaries of the current status of the subject of dynamic crack propagation can be found in recent review articles by Achenbach [1] and Freund [2]. In Refs. 1 and 2 several analytical solutions of linear elasto-dynamic equations for crack propagation in plane bodies with infinite domains have been reviewed. For finite bodies containing cracks and subjected to time-dependent loading, the interaction with a crack-tip of stress-waves reflected from the boundaries and/or emanated by the other moving crack-tip play an important role in determing the intensity of the dynamic singular stress-field at the considered crack-tip. Because of the analytical intractability of such elasto-dynamic problems for finite domains, computational techniques are

*Research Scientist
**Regents' Professor of Mechanics, Member ASME

mandatory. A critical appraisal of several different numerical (finite element and finite difference) techniques was made by Kanninen [3] in 1978. Most of the finite element methods reviewed in [3] use conventional assumed-displacement finite elements near the crack-tip and hence do not accout for the known crack-tip singularity. Moreover in these methods, crack-propagation is simulated by the well-known "node-release" technique, which was argued in [3] to be not sufficiently accurate. The literature an dynamic finite element methods for simulation of fast fracture, since the appearance of [3], has been reviewed in [4,5,6].

In Refs. [4,5,6] the authors have presented a "moving-singularity" finite element procedure for the analysis of dynamic crack propagation in arbitrarily shaped finite bodies. In this procedure a singular crack-tip element, within which a large number of analytical eigen-functions corresponding to a propagating crack [4,7] are used as basis functions for displacements, translates by an arbitrary amount $\Delta\Sigma$ in each time-increment Δt of the numerical time-integration procedure. The moving crack-tip singular-element, within which the crack-tip always has a fixed location, retains its shape at all times, but the mesh of conventional (isoparametric) finite elements, surrounding the moving singular-element, deforms accordingly. An energy-consistent variational statement was developed in [4,5,6] as a basis for the above moving singularity procedure. It was also shown in [4,5,6] that the procedure there in lead to a direct evaluation of the dynamic stress-intensity factors for propagating cracks. Several numerical studies were presented in [4,6] to illustrate the relative efficiency of the above procedure as compared to the "node-release" techniques reviewed in [3,4].

In the present paper we present further numerical results for the problem of dynamic propagation, at different constant velocities, of a centrally located crack in a square panel. These results augment the pre-

liminary conclusions reached in [4,6] concerning the effects of interactions of stress-waves emanated from a moving crack-tip and those reflected from the boundaries of the panel on the dynamic stress-intensity factor at the considered crack-tip. These results are also shown to lead to a simple formula for estimating the dynamic K factor in similar situations. Also presented are the results of simulation of data on the crack-tip velocity history in an experiment on a double-cantilever-beam specimen reported by Kalthoff et al [8]. The dynamic stress-intensity factors, for this specimen, computed from the present procedure are compared with the experimentally determined data of [8], and independent numerical results of Kobayashi et al [9] and Popelar et al [10], and pertinent discussions are presented.

In the second part of the paper, results of an investigation of the stress-intensity factors near the border of a meridional semi-elliptical surface flaw at the inner surface of a cylindrical pressure vessel which is subjected to a thermal shock, are presented. The presently reported results are obtained by using "three-dimensional hybrid crack-elements" near the crack front, the development of which was reported eariler by the authors [11,12,13]. The present results are compared with those reported earlier by Kobayashi et al [14].

Part I. Dynamic Crack Propagation Analysis

Synopsis of the Analysis Procedure: In the procedure adopted in the paper, the basis functions used for displacement, velocity, and acceleration in the crack-tip "singular element" are:

$$u_\alpha(\xi,x_2,t) = u_{\alpha j}(\xi,x_2,v)\beta_j(t) \quad [\alpha=1,2 \; ; \; j=1,\ldots N] \tag{1}$$

$$\dot{u}_\alpha = u_{\alpha j}\dot{\beta}_j - v\, u_{\alpha j,\xi}\, \beta_j \tag{2}$$

$$\ddot{u}_\alpha = u_{\alpha j}\ddot{\beta}_j - 2- u_{\alpha j,\xi}\dot{\beta}_j + v^2\, u_{\alpha j,\xi\xi}\,\beta_j \qquad (3)$$

where $u_{\alpha j}$ correspond to the "steady-state" (ie., which are invariant to an observer moving with the crack-tip) eigen-function solutions for the elasto-dynamic wave equations (with independent variables ξ, and x_2) for crack propagation at constant velocity v in a plane domain. Note that $x_\alpha(\alpha=1,2)$ are fixed coordinates, with $x_2 = 0$ defining the crack plane and $\xi = x_1 - vt$. It is noted that the first term, viz., $u_{\alpha 1}$, leads to the appropriate $(r^{-1/2})$ type singularity in strains and stresses. The singular element in the present procedure is surrounded by the usual isoparametric [8-noded, in the present case] elements. The displacement compatibility between the singular element and the surrounding isoparametric elements is satisfied in the present analysis through a least-square technique.

Consider two instants of time, t_1 and $t_2 = t_1 + \Delta t$. Assume that in a mode I crack propagation problem, the crack-lengths ar t_1 and t_2 are, respectively, Σ_1 and $\Sigma_1 + \Delta\Sigma$. Let the displacements, strains, and stresses at t_1 be denoted by u_i^1, ε_{ij}^1, and σ_{ij}^1, respectively, while those at t_2 are denoted by a superscript <u>two</u> for each variable. The variables at time t_1 are pressumed to be known. It has been shown in [4,5] that the variational principle governing the dynamic crack propagation between times t_1 and t_2 can be written as:

$$\int_{V_2} (\sigma_{ij}^2 + \sigma_{ij}^1)\delta\varepsilon_{ij}^2 + \rho(\ddot{u}_i^1 + \ddot{u}_i^2)\delta u_i^2\, dV$$

$$= \int_{S_{\sigma_2}} (\bar{T}_i^1 + \bar{T}_i^2)\delta u_i^2\, ds + \int_{\Sigma_1^+} (\bar{T}_i^2 + \bar{T}_i^1)^+(\delta u_i^2)^+$$

$$+ \int_{\Delta\Sigma^+} (\bar{T}_i^2 + \sigma_{ij}^1\, \nu_j^1)^+(\delta u_i^2)^+\, ds \qquad (4$$

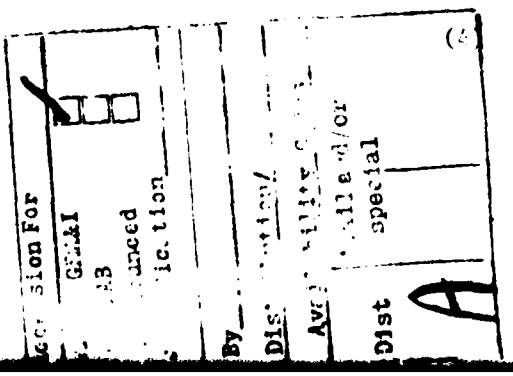

where V_2 is the domain of the body, and S_{σ_2} is the boundary of V_2 where tractions are prescribed, at time t_2. $\bar{T}_i^1$ are the prescribed tractions at time t_1 at S_{σ_1} ($\subseteq S_{\sigma_2}$) and $\bar{T}_i^2$ are the prescribed tractions at S_{σ_2} as well as at the newly created crack surface $\Delta\Sigma$ at time t_2. It is seen that $\sigma_{ij}^1 \nu_j^1$ at $\Delta\Sigma$ are the cohesive forces holding the crack-faces together at time t_1. In the above, mode I conditions are assumed; hence, only the upper half of the domain with the crack face Σ^+ is considered.

In the variational principle in Eq. (4), the varialbes $\ddot{u}_i^1$, and σ_{ij}^1 are pressumed known; while σ_{ij}^2, ε_{ij}^2, and u_j^2 are the variables. The variables u_j^2 are assumed according to Eq. (1), with the velocity v_2 appearing in them. Further, the variational principle in Eq. (4) is used to develop a discrete (finite element) approximation for a (finite element) mesh at time t_2. Note that at time t_2, in the present problem, the crack-tip is located at $x = \Sigma_1 + \Delta\Sigma$ and hence the present crack-element is centered at $x_1 = \Sigma_1 + \Delta\Sigma$. In developing the equations for the finite element mesh at t_2, it is seen from Eq. (4), that the variation of σ_{ij}^1 and u_j^1 must be known in the finite element mesh at time t_2. However, σ_{ij}^1 and u_j^1, and $\ddot{u}_j^1$ were solved for, in the finite element mesh at t_1. In the mesh at t_1 the crack-tip is located at $x_1 = \Sigma_1$ and hence the crack-element is centered at Σ_1. Thus, between t_1 and t_2 ($= t_1 + \Delta t$) the crack-element is translated by an amount $\Delta\Sigma$. While the crack-element is translated, only the elements immediately surrounding the moving crack-tip are distorted. Thus the finite element meshes at times t_1 and t_2 differ only in the location of crack-tip (and hence the crack-element) and the shapes of the immediately surrounding isoparametric elements. Thus, the known data for σ_{ij}^1 and u_j^1 in the mesh at t_1 is interpolated easily into corresponding data in the mesh at t_2. Based on these concepts, the development of the finite-element equations from the principle in Eq. (4), and the numerical integration of these equations follows the well-established procedures. Further details

can be found in [4,5] where it is shown that the dynamic k-factors can be computed directly in the present analysis procedure.

Propagation of a Central Crack in a Square Panel

In Ref. [6], the problem of a centrally cracked square panel (L=W=40mm) [with material properties: μ(shear modulus) = 2.94×10^{10} N/mm^2; ν(Poisson ratio) = 0.286; and ρ(mass density) = 2.45×10^3 Kg/m^3], which was subject to time-independent tensile stress at the edges of the specimen parrellel to the crack axis, was considered. The crack was assumed to start propagating from an initial length, $\Sigma_o/W = 0.2$, and to grow symmetrically with a constant velocity v. Four different cases of v, namely, $(v/C_s) = 0.2$, 0.4, 0.6 and 0.8, respectively (where C_s is the shear wave speed) were considered. These limited results appeared to suggest a simple formula to estimate the dynamic stress-intensity factor in such problems. Until the time ($t=R_c$) taken by the Rayliegh waves emanating one crack-tip to interact with the other moving crack-tip, the dynamic stress intensity factor was noted in [6] to be given approximately by the equation:

$$K_d = F(\Sigma_o)\, K^{*\infty}(\Sigma)\, k(v) \qquad t < R_c \tag{5}$$

where $F(\Sigma_o)$ is the finite size correction factor in the static stress intensity factor K_s for the given geometry and loading at a crack length Σ_o; $K^{*\infty}$ is the static factor (which, in general, is not equal to the static stress-intensity factor K_s^{∞}) for an infinite body subjected to uniform stress normal to crack axis; and k(v) is a universal velocity factor. The expressions for $K^{*\infty}$ and k(v) were given by Eshelby [15], and Broberg [16] respectively. After the time $t = R_c$, the dynamic stress-intensity factor was found in [6] to be given by the approximate relation:

$$K_d = \beta\, K_s^f\,(\Sigma)\; K(v) \qquad t > R_c \tag{6}$$

where $$\beta = [F(\Sigma_o)\; K^{*\infty}(\Sigma)]/[K_s^f(\Sigma)] \text{ at } \Sigma = \Sigma_{RC}$$

where K_s^f is the static stress-intensity factor for the present finite domain and Σ_{RC} is the current crack length at $t = R_c$. It is seen that

$$\Sigma_{RC} = \Sigma_o + v\,(2\Sigma_o)/(C_R - v) \tag{7}$$

where C_R is the Rayleigh wave speed.

Here we present further results for the case when a central crack in a square panel starts from an initial length of $(\Sigma_o/W) = 0.1$ and propagates with a constant velocity v. Two cases of v, namely, $(v/C_s) = 0.1$ and 0.2, respectively, are considered.

The finite element mesh at the initial crack length Σ_o, for a quadrant of the panel (which only is modelled due to symmetry), is shown in Fig. 1. This mesh has 262 nodes and 564 degrees of freedom before the imposition of the appropriate symmetry conditions at the boundaries. The computed results for the normalized dynamic stress-intensity factor (normalized by $\sigma\sqrt{\pi\Sigma}$, Σ being the current crack length) are shown in Fig. 2.

For the present material, $(C_R/C_S) = 0.9238$. Thus it is seen from Eq. (7) that for the present cases of $(\Sigma_o/W) = 0.1$, and $(v/C_s) = 0.1$ and 0.2, one obtains $(\Sigma_{Rc}/W) \simeq .12$, and .15, respectively. Shown in Fig. (2) are the curves: (i) the normalized static-stress-intensity factor K_s^f; (ii) the presently computed normalized dynamic stress-intensity factor; and (iii) the approximations for the dynamic-stress intensity factor as given by Eqs. (6) and (7).

It is seen that the correlation between the directly computed dynamic K-factor and that obtained from the simple approximations in Eqs. (6) and (7) is very good. Approximate formulae similar to those given in Eq. (6) and (7)

for the more common dynamic fracture test specimens such as the double cantilever specimen, wedge-loaded single edge notch specimen, and modified compact tension specimen would greatly aid in the estimation of dynamic K-factors from the experimentally obtained data for $\Sigma(t)$ and/or $d\Sigma/dt$. Such studies are currently underway and will be reported elsewhere.

Rectangular Double Cantilever Specimen

The geometry of one-half of the specimen is shown in Fig. 3 along with the details of the finite element mesh used in the present analysis. Only the static material properties E = 3380 MN/m^2 and ν = 0.33 for the present Araldite B material are used in the present analysis, partly due to the reason of comparing the present results with those of Kobayashi [9]. The presently used boundary conditions are similar to those in [9]. The experimental data for crack-length (Σ) versus time history that is simulated in the present analysis corresponds to specimen No. 4 reported by Kalthoff et al [8]. In reference [8], the crack-initiation stress-intensity factor, K_{Iq}, which was computed fom the experimentally measured deflection 2δ at the loading points by using the formula of Kanninen [17], was quoted as 2.32 $MN/m^{3/2}$. However, the value of δ was not quoted in [8]. By using the formula in [17], the load point deflection to create an initiation K-factor of 2.32 is calculated to be δ_k. However, in the present finite element method, a load point deflection of (1.1) δ_k was found necessary to impose the K_{Iq} value of 2.32 $MN/m^{3/2}$ on the model. This discrepancy may be due to the approximate nature of the analysis in [17].

The crack-length versus time history (Σ vs. t) for specimen No. 4 reported in [8] shown is Fig. 4. The crack-tip-velocity versus time [$\dot{\Sigma}$ vs. t] curve, obtained by numerically differentcating the (Σ vs. t) curve is also shown in Fig. 4, and is seen to be in good agreement with that shown in Fig. 6 of [8].

Kalthoff et al [8] measure the dynamic stress-intensity factors by applying the method of caustics. However in [8], the relation between the diameter D of the caustic and the stress-intensity factor, is based on the static solution for the stress-strain field around the tip of the crack. However, Beinert et al [18] show that if the above relation is derived from a dynamic solution for the stress-strain field around the crack, the thus computed K-factors may defer from those in [8] by a factor [1/F]. It is noted that only the basic singular dynamic plane stress solution is used in developing the relation between K_I and D. It was estimated in [18] that F = 1.095 for v = 500 m/s, and F = 1.028 for v = 300 m/s, where v is crack-tip velocity. Further it is noted that the epoxy resin Araldite B is a viscoelastic material whose properties are rate-dependent. However, in the present analysis as well as in [18] the material is modeled as linear elastic through out.

It is seen from Fig. 4 that the presently computed dynamic K-factor, K_d, agrees well with the experimental data [roughly to within the above discussed factor (1/F)] until the time when the crack-tip begins to decelerate as per the $\dot{\Sigma}(t)$ curve (which is obtained by numerical differentiation of the the experimental data for $\Sigma(t)$). In the time interval between the beginning of crack-tip deceleration and its' eventual arrest, significant differences are noted between the present results for K_d and those reported in [8].

To understand the above descrepancies in the results of Fig. 4, and to study the effect of small changes in the assumed Σ versus t curve, the analysis was repeated for three different cases of assumed $\Sigma(t)$ curves as shown in Fig. (5). It is seen that the curves in Fig. (5) represent minor deviations from the "experimental" data reported in [8]. It is also noted that the $\Sigma(t)$ curve marked as "Data 3" is identical to the one used by Kobayashi et al [9] in their "generation" [9] calculation. The presently computed K_d curves,

for each of the three assumed Data for $\Sigma(t)$ in Fig. (5), are shown in Fig. (6). Also shown in Fig. (6) are the $\dot{\Sigma}(t)$ curves corresponding to each of the assumed $\Sigma(t)$ curves, with the curve for 'Data 3' being similar to that in [9]. The results for K_d computed by Kobayashi in his "generation" calculation [9] and the experimental results of [8] are also shown in Fig. (6). It is seen that significant differences exist between the present results for each of the three $\Sigma(t)$ data cases, and those in [8], during roughly the last third of the crack-propagation history. Each of the three curves, for present results, shown in Fig. (6) exhibit a pronounced maximum during the later third of crack-propagation history. The results of Kobayashi [9] also exhibit a pronounced maximum for K_d, which however is seen to occur earlier than in each of the present three cases.

Such differences, compared to the experimental data, as in Fig. 6, were also noted even in the "propagation" calculations (in the sense defined in [9]) by Kobayashi [9], and Popelar et al [10].

It is seen from Fig. (6) that the maximum value of the presently computed K_d is the largest for "Data 3" while it is smallest for Data 1. Note that the rate of crack-tip deceleration is the most severe for Data 3, while for Data 1, the deceleration is zero, ie., the crack-tip is still propagating with a constant velocity of 295 m/sec. Thus, the more severe the crack-tip deceleration is, the more higher is the maximum in the computed K_d. To understand the reasons for the peak in K_d for Data 1, the times for various waves, reflected from the boundaries, to interact with the propagating crack-tip are computed and shown in Fig. (6). With A, B, and C denoting the three boundaries as marked in Fig. 3, D_A, D_B and D_C are the times when the dilatational waves reflected from the boundaries A, B, and C, respectively, interact with the propagating crack-tip. Likewise, S_A and S_B are the times for the shear waves

reflected from boundaries A and B, respectively, to interact with the moving crack-tip. It is interesting to note that the computed K_d, for the Data 1 case, begins to peak at the instant S_B. Further, the present analysis procedure has been found to yield excellent correlations in several constant as well as non-constant velocity propagation problems, such as those of Broberg, Freund, and Nillson, in [6]. Thus it appears reasonable to conclude that the results in Fig. 6 for Data 1 may be accurate.

To further understand the validity of the results for the most severe case of Data 3, the variations of strain energy (U), the kinetic energy (T), the fracture energy (F) and the total input energy (W) were studied for the case of Data 3 (which as seen in Fig. 6, results in the most serious descrepancy with the cited experimental results). It is noted that in the present analysis procedure, the dynamic stress-intensity factor K_d is calculated directly as a variable in the finite element equations [4,5]. The fracture energy is computed from this directly computed K_d factor, using the relations;

$$F = \int_{\Sigma_o}^{\Sigma} G \, d\Sigma \tag{8}$$

where $$G = \frac{S_1(1-S_2^2)}{4S_1S_2-(1+S_2^2)} \qquad \frac{K_d^2}{2\mu}$$

$$S_j = [1-(v/C_j)^2]^{1/2}$$

In Eq. (8), C_1 and C_2 are the dilatational and shear wave speeds respectively. The strain energy U is calculated from the presently computed stress and strain data, while the kinetic energy is calculated from the computed data for velocities. Since the input energy to the specimen, W, is a constant in the present case, the above computed F, U, and T should add up to a constant. It is seen that the error in (F + U + T) as compared W increases almost linearly from 0.0% to

about 4.5% towards the end of the computation. Since the present calculation was carried out in 165 time-steps, it is reasonable to presume that the error in each time step is thus, roughly 0.0003%. This appears to give enough credence to the presently computed K_d for the case of Data 3, as in Fig. 6.

The results in Fig. 4 and 6 indicate the sensitivity of computed K_d, in a generation calculation (in the sense defined in [9]), to the input data for the crack-tip time history, Σ vs. t. This in turn points to the extreme precision with which the history $\Sigma(t)$ should be determined in an experimental measurement. Also, the validity of using only the basic singular dynamic plane-stress solution in developing the relation between K and the caustic-diameter as in [18] appears to need further study.

The reason for the descrepancies in the presently computed results and the experimental ones for K_d, as in Figs. (4) and (6) may be explained, in part, by the fact that only the elastic strain energy, kinetic energy, and fracture energy are considered in an energy balance relation, of the type shown in Fig. 7, in the present procedure based on a linear-elastic rate-independent material. However for viscoelastic resins of the type of Araldite B used in the experiments [8], the viscous dissipation of energy may also play an important role in the determination of K_d. This may distort the comparison of such experimental results, and the computational results based on a linear elastic material behaviour.

Part II. Thermally Shocked Cylinder with Meridional Inner Surface Flaw

Synopsis of the Method of Approach: Special three-dimensional hybrid crack elements are used to model the immediate vicinity of the three-dimensional crack front, and the conventional 20-noded isoparametric brick elements are used to model the remainder of the cylinder. The special crack elements are developed through a hybrid displacement finite element procedure.

Thus, the development of the hybrid crack elements is based on a three field variational principle [11,12] with the arbitrary displacements in the interior of the element, a displacement field at the boundary of the element, and a Lagrange multiplier field which can be identified as the traction field at the boundary of the element, as the three variables. The analytical asymptotic solutions for the displacement field, under mixed mode (K_I, K_{II}, K_{III}) conditions, is embedded in the assumed interior displacement field of the crack-element. The boundary displacement field for the crack element is assumed such that it is inherently compatible with that of the surrounding conventional element. The third field, namely, the boundary traction field of the crack element, which is the Lagrange multiplier to enforce the equality of the boundary-value of the assumed interior displacement field and the independently assumed boundary-displacement field of the crack element, is assumed such that it includes the proper (1/ r) singularities near the crack front. From the details of the present finite element procedure [11,12,13] it can be seen that the mixed mode stress-intensity factors (K_I, K_{II}, and K_{III}) at various points along the crack front (which are denoted by a master vector $\underset{\sim}{k}^*_s$) can be solved for directly from the final finite element equations:

$$\underset{\approx}{K}_1 \underset{\sim}{q}^* + \underset{\approx}{K}_2^T \underset{\sim}{k}^*_s = \underset{\sim}{Q}_1 \tag{9}$$

$$\underset{\approx}{K}_2 \underset{\sim}{q}^* + \underset{\approx}{K}_3 \underset{\sim}{k}^*_s = \underset{\sim}{Q}_2 \tag{10}$$

where $\underset{\approx}{K}_i$ (i=1...3) are the corresponding global stiffnesses and $\underset{\sim}{Q}_\alpha$ (α=1,2) are the corresponding nodal forces.

Results

The above described hybrid crack element procedure was applied to analyse a thermally shocked cylindrical vessel, of commerical geometry with outer to inner radii ratio of (R_o/R_i) = (10/9), and containing an inner surface elliptical

flaw. The flaw parameters are: $(a/c) = 0.2$; $a/(R_o-R_i) = 0.6$; where the parameters are defined in Fig. 8. The initial temparature of the vessel is T_i and inner surface of the vessel is assumed to be instantaneously reduced to a temparature of T_E. The transient temparature distribution in the cylinder is obtained from [14] as:

$$\frac{T-T_E}{T_i-T_E} = -\pi \sum_{m=1}^{\infty} e^{-K\alpha_m^2 t} \frac{J_o(R_i\alpha_m)J_o(R_o\alpha_m)U_o(r\alpha_m)}{J_o^2(R_i\alpha_m) - J_o^2(R_o\alpha_m)} + \frac{\ln(r/R_i)}{\ln(R_o/R_i)} \qquad (11)$$

where $U_o(r\alpha_m) = J_o(r\alpha_m)Y_o(R_o\alpha_m) - J_o(R_o\alpha_m)Y_o(r\alpha_m)$; J_o and Y_o are Bessel functions of the first and second kind, respectively; α_m are the roots of $U_o(R_i\alpha_m) = 0$; K is the thermal diffusivity; and t is the time. For purposes of normalizing the final solution stress-intensity factors, the maximum value of non-dimensional hoop stress $\sigma_o = [(\sigma_{\phi\phi})_{max}]/[E\alpha(T_i-T_E)]$ is taken from [14] to be 5.1755 (where E and α are the modulus of elasticity, and the coefficient of thermal expansion, respectively).

One fourth of the vessel is modeled, and the finite element breakdown, which is shown in Fig. 9, consists of 380 elements and about 5600 degrees of freedom. The solution for stress-intensity factors for a semielliptical surface flaw, with $(a/c) = 0.2$ and $a/(R_o-R_i) = 0.6$, is shown in Fig. 10 along with the comparison results from [14]. In the normalization of the stress-intensity factors, the normalizing factor σ_o, which is defined earlier, is used. Thus the results presented in Fig. 10 would have a unit of stress. Further, the ratio (Kt/R_i^2) is assumed to be 0.0001 in the present problem. The present solution is seen to differ from that in [14] by about 10% at the free surface ($\theta = 0°$) of the flaw.

However, this correlation can be considered to be good for purposes of practical application of an engineering fracture theory. From the present results, as well as the additional results present in [13], it is concluded that the

approximate "alternating-technique" solution presented in [14] may be adequate for an engineering analysis of thermally shocked, flawed, cylindrical pressure vessels.

Closure

Novel numerical techniques for the analysis of two-dimensional fast fracture situations, and three-dimensional static analysis of surface-flawed pressure vessels, have been presented and illustrated through solutions of certain important problems in both problem areas. The present numerical simulation of experimental data on a double-cantilever-beam specimen pointed to the need for highly sophisticated experimental measurement of crack-tip velocity history, as well as the need for the incorporation of more realistic material property data (for experimentally used viscoelastic resins such as Araldite B) in a computational scheme. Despite the tremondons advances made both in numerical as well as experimental techniques, much needs to be perfected in both the areas!

Acknowledgements

The work reported herein has been supported, in the most part, by the Office of Naval Research under Contract No. N0004-78-0636 with Georgia Tech. The authors thank Dr. N. Perrone for his encouragement. Thanks also go to Mrs. T. Rapp for her able typing of this manuscript.

References

[1] Achenbach, J. D., "Dynamic Effects in Brittle Fracture" in Mechanics Today, Vol. 1 (S. Nemat-Nasser, Ed.) 1972, Pergamon, 1972, pp. 1-57.

[2] Freund, L. B., "Dynamic Crack Propagation", in The Mechanics of Fracture, (F. Erdogan, Ed.) ASME-AMD Vol. 19, ASME, New York, 1976, pp. 105-134.

[3] Kanninen, M. F., "A Critical Appraisal of Solution Techniques in Dynamic Fracture Mechanics", in Numerical Methods in Fracture Mechanics (A. R. Luxmore and D. R. J. Owen, Eds.) Swansea, United Kingdom, 1978, pp. 612-634.

[4] Atluri, S. N., Nishioka, T., and Nakagaki, M., "Numerical Modeling of Dynamic and Nonlinear Crack Propagation in Finite Bodies, By Moving Singular Elements" in Nonlinear and Dynamic Fracture Mechanics, ASME-AMD Vol. 35 (N. Perrone and S. N. Atluri, Eds.) ASME, New York, 1979, pp. 37-67.

[5] Nishioka, T. and Atluri, S. N., "Numerical Modeling of Dynamic Crack Propagation in Finite Bodies, By Moving Singular Elements - Part I. Fromulation", Journal of Applied Mechanics 1979, (In review).

[6] Nishioka, T. and Atluri, S. N., "Numerical Modeling of Dynamic Crack Propagation in Finite Bodies, By Moving Singular Elements - Part II. Results", Journal of Applied Mechanics 1979, (In review).

[7] Malluck, J. F., "Crack Propagation in Finite Bodies", Ph.D. Thesis, Georgia Institute of Technology, 1976.

[8] Kalthoff, J. F., Beinert, J. and Winkler, S., "Measurements of Dynamic Stress Intensity Factors for Fast Running and Arresting Cracks in Double-Cantilever-Beam Specimens" Fast Fracture and Crack Arrest ASTM STP 627 (G. T. Hahn and M. F. Kanninen, Eds.) ASTM, 1977, pp. 161-176.

[9] Kobayashi, A. S., "Dynamic Fracture Analysis by Dynamic Finite Element Method-Generation and Propagation Analyses" in Nonlinear and Dynamic Fracture Mechanics ASME-AMD Vol. 35 (N. Perrone and S. N. Atluri, Eds.) ASME, New York, 1979, pp. 19-37.

[10] Popelar, C. H. and Gehlen, P. C., "Modeling of Dynamic Crack Propagation: II. Validation of Two-Dimensional Analysis", International Journal of Fracture, Vol. 15, No. 2, 1979, pp. 159-177.

[11] Kathiresan, K., "Three-Dimensional Linear Fracture Mechanics Analysis by a Displacement-Hybrid Finite Element Model", Ph.D. Thesis, Georgia Institute of Technology, 1976.

[12] Atluri, S. N. and Kathiresan, K., "3D Analysis of Surface Flaws in Thick-Walled Reactor Vessels Using Displacement-Hybrid Finite Element Method" Nuclear Engineering and Design, Vol. 51, No. 2, pp. 163-176.

[13] Kathiresan, K. and Atluri, S. N., "Natural Shaped Flaws at Nozzle Corners with Pressure Loading and Thermal Shock", 4th International Conference on Pressure Vessel Technology, London, May 1980 (to appear).

[14] Kobayashi, A. S., et al., "Surface Flaw in a Pressurized and Thermally Shocked Hallow Cylinder", International Journal of Pressure Vessels and Piping, Vol. 5, 1977, pp. 103-115.

[15] Eshelby, J. D., "The Elastic Field of a Crack Extending Non-Uniformly Under General Anti-plane Loading", Journal of Mechanical Physics of Solids, Vol. 17, 1969, pp. 177-199.

[16] Broberg, K. B., "The Propagation of a Brittle Crack", Arkiv För Physik, Band 18, No. 10, 1960, pp. 159-192.

[17] Kanninen, M. F., International Journal of Fracture, Vol. 9, No. 1, 1973, pp. 83-92.

[18] Beinert, J., Kalthoff, J. F. and Maier, M., "Neuere Ergbnisse Zur Anwendung des Schattenflekverfahrens auf stchende und Schnell-laufende Brüche", VDI-Berichte Nr. 313, 1978, pp. 791-798.

Number of Elements: 73

Number of Nodes: 262

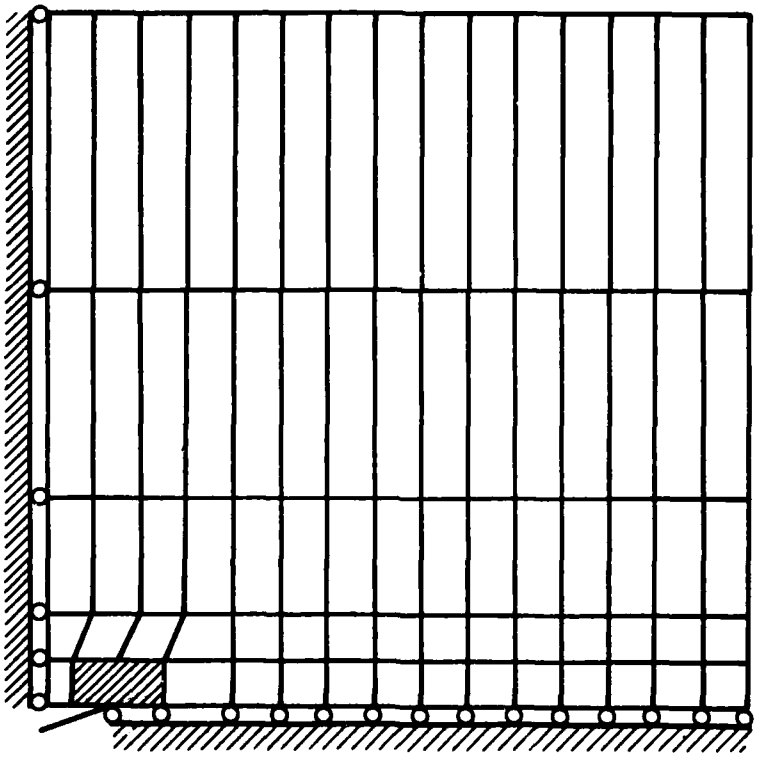

Fig. 1

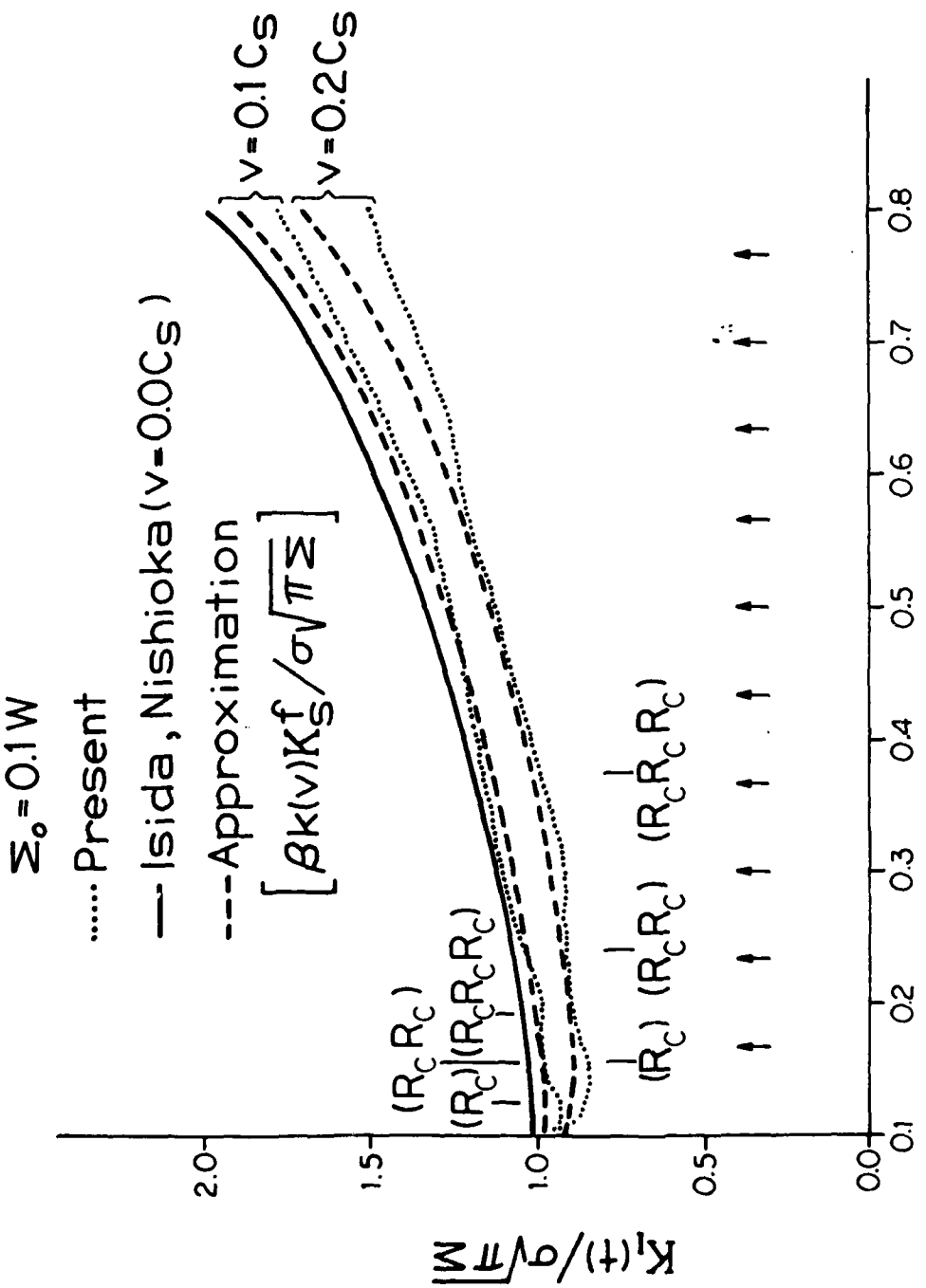
Σ_0=0.1W
.....Present
— Isida, Nishioka (v=0.0C_S)
---Approximation
$\left[\beta k(v) K_S^f / \sigma\sqrt{\pi\Sigma}\right]$
v=0.1C_S
v=0.2C_S
$(R_C R_C)$
$(R_C)(R_C R_C R_C)$
(R_C) $(R_C R_C)$ $(R_C R_C R_C)$
$K_I(t)/q\sqrt{\pi\Sigma}$
2.0
1.5
1.0
0.5
0.0
0.1
0.2
0.3
0.4
0.5
0.6
0.7
0.8
Σ/W

Fig. 2

L = 321.0 mm

H = 63.5 mm

Σ_o = 67.8 mm

	Static	Dynamic
E	3380	3660 MN/m^2
ν	0.33	0.39

(Static material constants are used)

Number of Nodes : 179

Number of Elements : 46

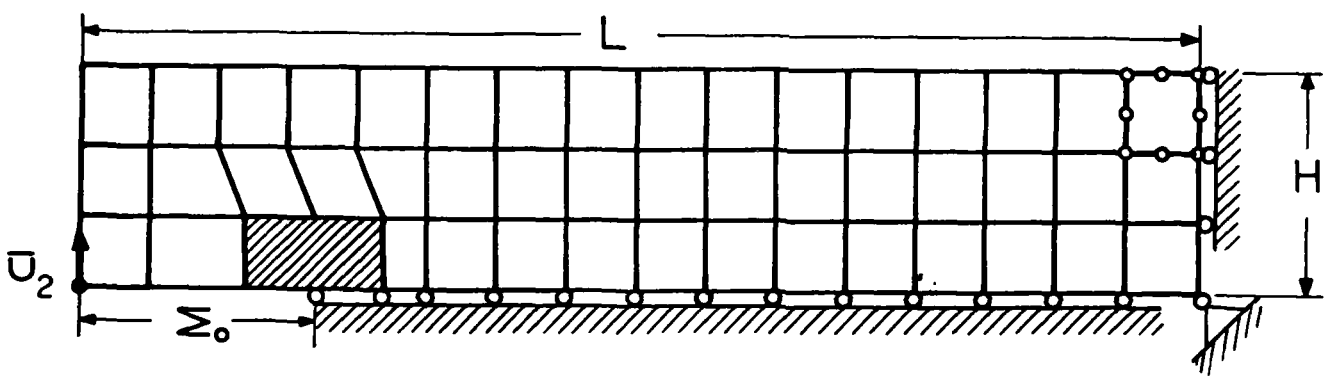

Fig. 3

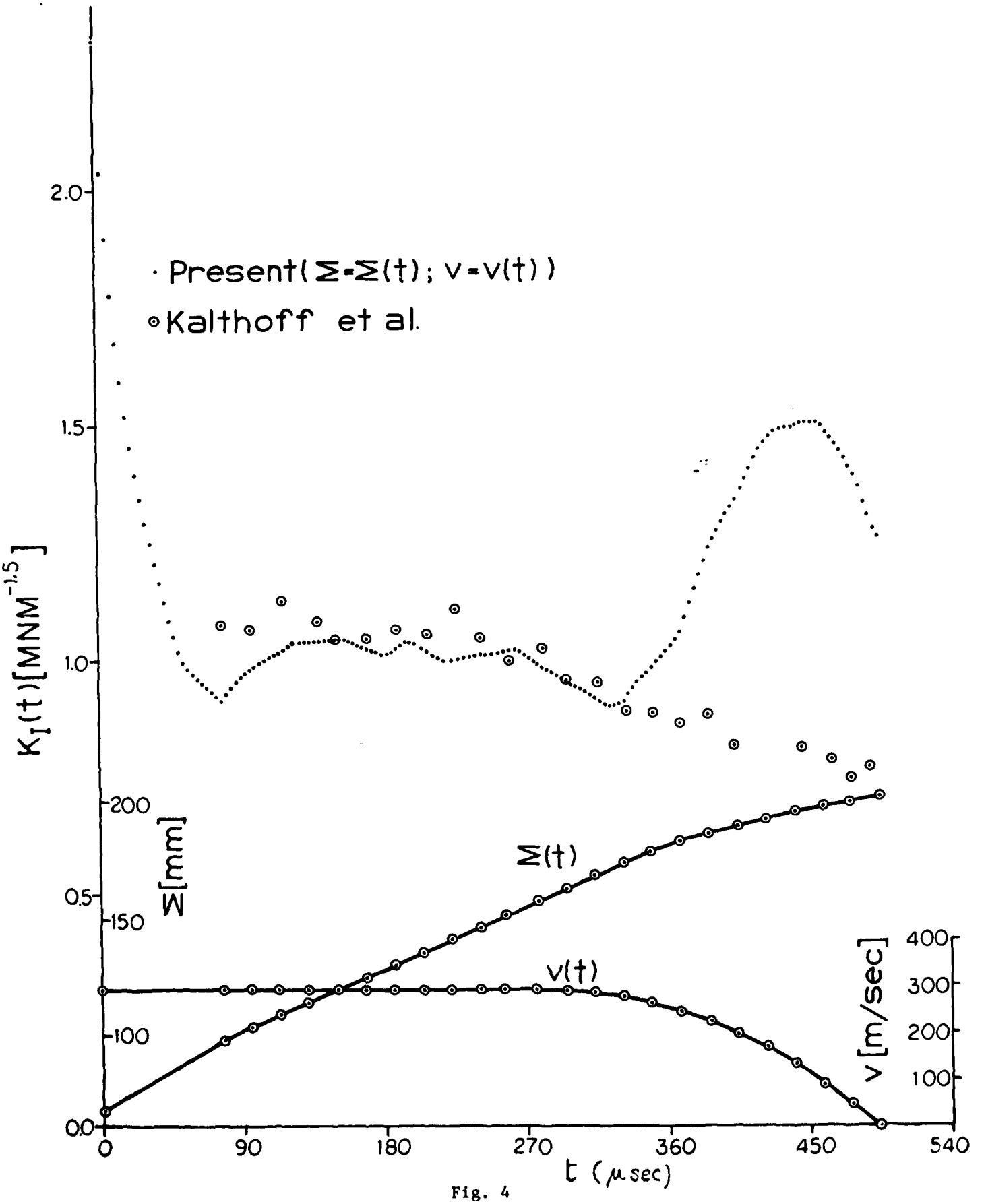
· Present(Σ=Σ(t); v=v(t))
⊙ Kalthoff et al.
$K_I(t)[MNM^{-1.5}]$
2.0
1.5
1.0
0.5
0.0
Σ[mm]
200
150
100
Σ(t)
v(t)
v [m/sec]
400
300
200
100
0
90
180
270
360
450
540
t (μsec)

Fig. 4

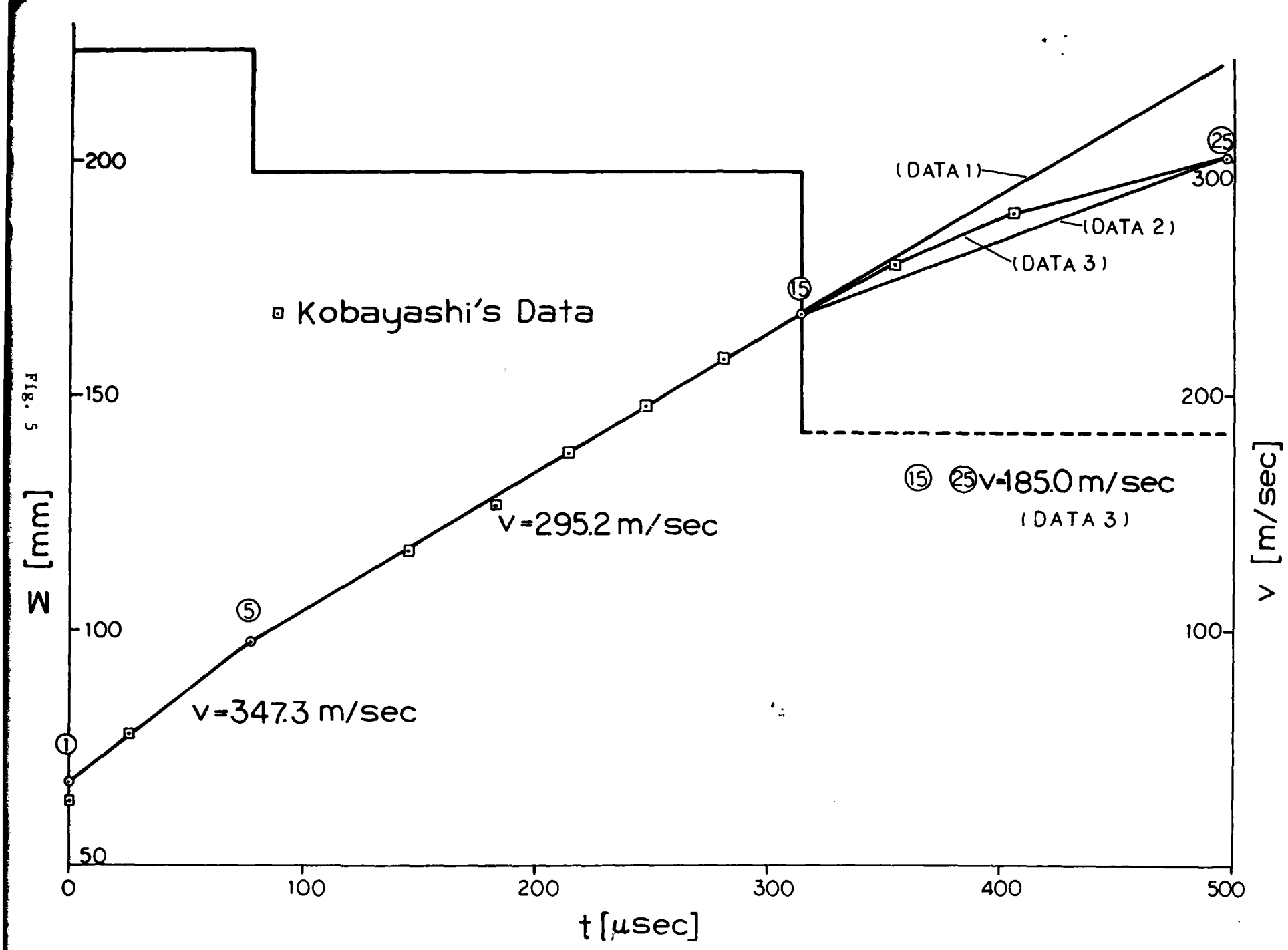
Kobayashi's Data
(DATA 1)
(DATA 2)
(DATA 3)
v=347.3 m/sec
v=295.2 m/sec
⑮ ㉕v=185.0 m/sec
(DATA 3)
W [mm]
v [m/sec]
t [μsec]
200
150
100
50
0
100
200
300
400
500
300
200
100
①
⑤
⑮
㉕

Fig. 5

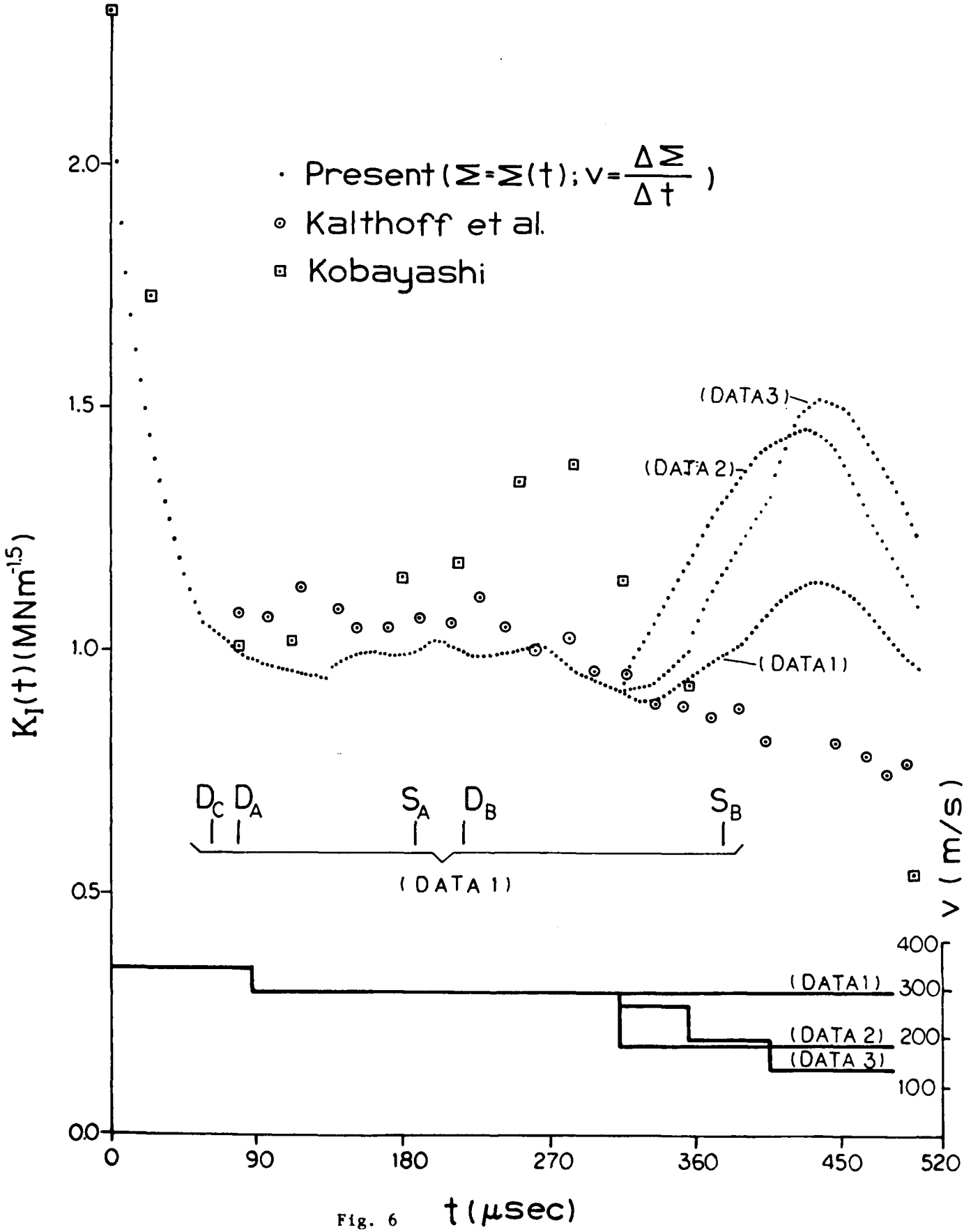
· Present ($\Sigma=\Sigma(t)$; $v=\frac{\Delta\Sigma}{\Delta t}$)
⊙ Kalthoff et al.
⊡ Kobayashi
(DATA3)
(DATA2)
(DATA1)
$K_I(t)$ (MNm$^{-1.5}$)
2.0
1.5
1.0
0.5
0.0
D_C D_A S_A D_B S_B
(DATA 1)
v (m/s)
400
300
200
100
(DATA1)
(DATA 2)
(DATA 3)
0
90
180
270
360
450
520
t (μsec)

Fig. 6

$$\left(\frac{U+T+F}{W}-1\right)_{165} = -4.58\%$$

$$\text{average} = \frac{-4.58\%}{165} = -0.00028\%$$

(Kalthoff No.4 Data 2)

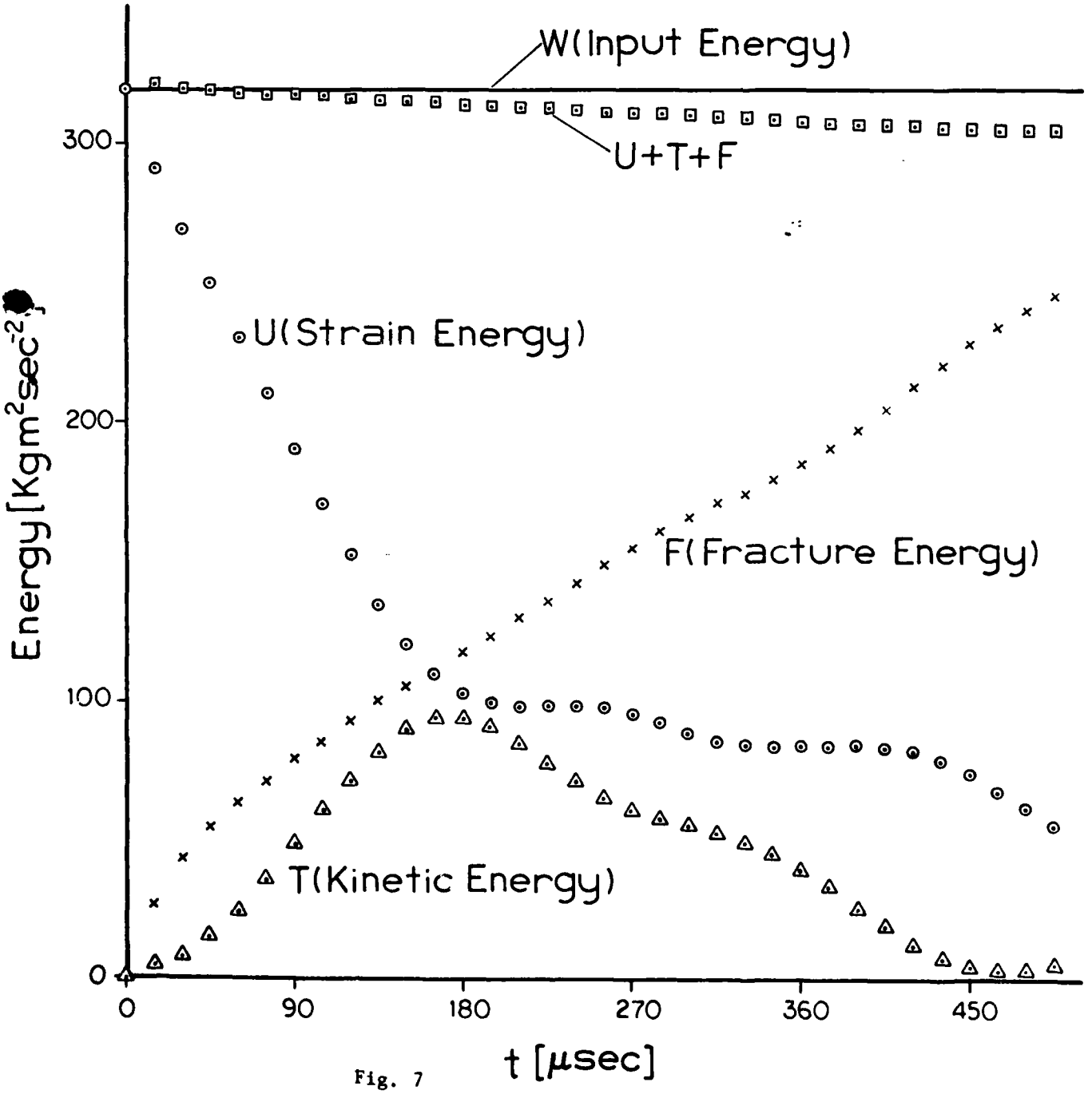

Fig. 7

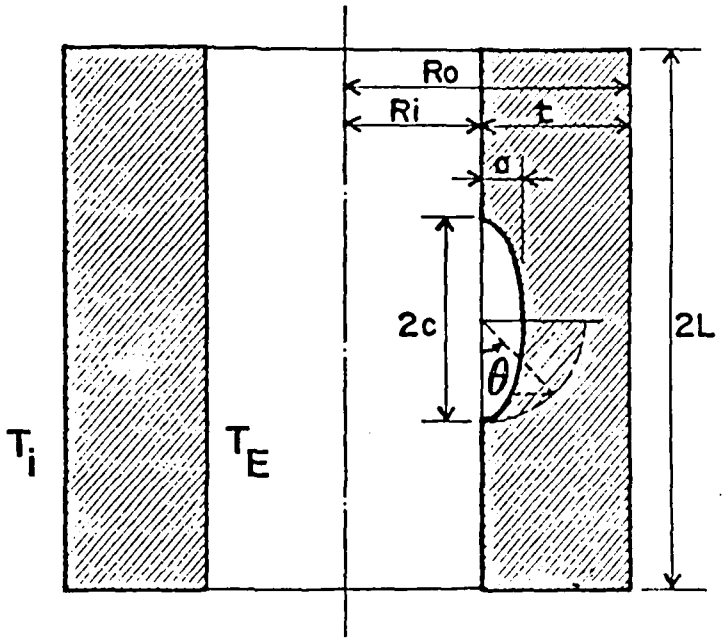

Fig. 8

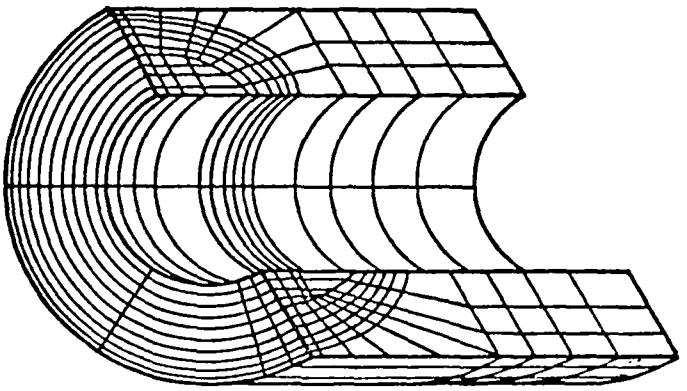

Fig. 9

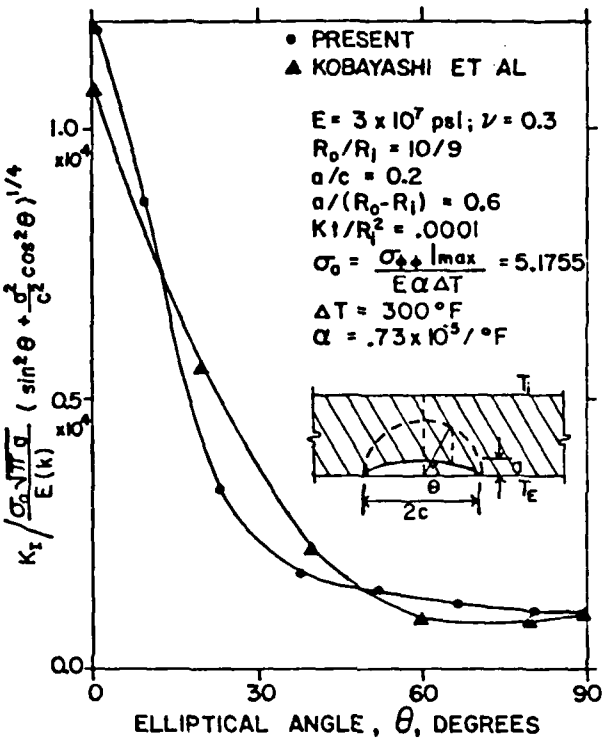
• PRESENT
▲ KOBAYASHI ET AL
E = 3 x 10^7 psi; ν = 0.3
R0/R1 = 10/9
a/c = 0.2
a/(R0-R1) = 0.6
K1/R1^2 = .0001
σ0 = σφφ |max / EαΔT = 5.1755
ΔT = 300°F
α = .73 x 10^-5 /°F
Ti
θ
2c
Te
1.0
x10^4
0.5
x10^4
0.0
0
30
60
90
ELLIPTICAL ANGLE, θ, DEGREES

Fig. 10

Figure Captions

Fig. 1 Finite element model for a center-cracked panel.
Propagating singularity element is shown my hatched markings.

Fig. 2 Normalized dynamic stress intensity factor variation with $\Sigma(t)$.

Fig. 3 Finite Element Model for a Double-Cantilever-Beam Specimen.

Fig. 4 Normalized dynamic stress-intensity factor as a function of time, with Kalthoffs $\Sigma(t)$ curve as input.

Fig. 5 Three different $\Sigma(t)$ curves assumed in the analysis.

Fig. 6 Normalized dynamic stress-intensity factor as a function of time, for each of the three assumed $\Sigma(t)$ curves.

Fig. 7 The variation with time of different energies in the specimen.

Fig. 8 Nomenclature for a thermally shocked, internally cracked cylinder.

Fig. 9 Finite element breakdown for the crack cylinder.

Fig. 10 Stress-intensity factor variation along the flaw-border for a thermally shocked cylinder.

SECURITY CLASSIFICATION OF THIS PAGE (When Data Entered)

REPORT DOCUMENTATION PAGE	READ INSTRUCTIONS BEFORE COMPLETING FORM
1. REPORT NUMBER: GIT-CACM-SNA-20	2. GOVT ACCESSION NO.: AD-A087 225
	3. RECIPIENT'S CATALOG NUMBER:
4. TITLE (and Subtitle): Efficient Computational Techniques for the Analysis of Some Problems of Fracture in Pressure Vessels and Piping	5. TYPE OF REPORT & PERIOD COVERED: Interim Report
	6. PERFORMING ORG. REPORT NUMBER: GIT-CACM-SNA-20
7. AUTHOR(s): T. Nishioka and Satya N. Atluri	8. CONTRACT OR GRANT NUMBER(s): N00014-78-C-0636
9. PERFORMING ORGANIZATION NAME AND ADDRESS: Center for the Advancement of Computational Mechanics, School of Civil Engineering, Georgia Institute of Technology, Atlanta, GA 30332	10. PROGRAM ELEMENT, PROJECT, TASK AREA & WORK UNIT NUMBERS: NR 064-610
11. CONTROLLING OFFICE NAME AND ADDRESS: Office of Naval Research, Structural Mechanics Program, Dept. of the Navy, Arlington, VA 22217	12. REPORT DATE: June 1980
	13. NUMBER OF PAGES: 28
14. MONITORING AGENCY NAME & ADDRESS(if different from Controlling Office)	15. SECURITY CLASS. (of this report): Unclassified
	15a. DECLASSIFICATION/DOWNGRADING SCHEDULE

16. DISTRIBUTION STATEMENT (of this Report)

Unlimited

This document has been approved for public release and sale; its distribution is unlimited.

17. DISTRIBUTION STATEMENT (of the abstract entered in Block 20, if different from Report)

18. SUPPLEMENTARY NOTES

ASME Paper No. 80-C2/PVP-10, Century 2 Emerging Technology Conference, Aug. 10-21, 1980
San Francisco

19. KEY WORDS (Continue on reverse side if necessary and identify by block number)

Dynamic Fracture, Crack Propagation, Crack Arrest, Moving Singularities

20. ABSTRACT (Continue on reverse side if necessary and identify by block number) Results of (i) a numerical investigation, based on an energy consistent moving-singularity dynamic finite element procedure, of fast crack propagation in a finite plate; (ii) numerical simulation of experimental data on fast crack propagation and arrest in a double-cantilever-beam specimen; and (iii) stress-intensity factor solutions in a thermally shocked cylindrical vessel containing an inner surface (meridional) elliptical flaw, are presented. Comparison of these results with other available solutions, and pertinant discussions, are included.

DD FORM 1 JAN 73 1473 EDITION OF 1 NOV 65 IS OBSOLETE

Unclassified

SECURITY CLASSIFICATION OF THIS PAGE (When Data Entered)